Journal of Organometallic Chemistry 693 (2008) 3797–3809

Contents lists available at ScienceDirect

Journal of Organometallic Chemistry

journal homepage: www.elsevier.com/locate/jorganchem

Tunable electronic coupling in iron–chromium mixed-valence ions of methylated Cp-indene ligands

Saverio Santi [a,*], Laura Orian [a], Alessandro Donoli [a], Christian Durante [a], Annalisa Bisello [a], Marilena Di Valentin [a], Paolo Ganis [a], Franco Benetollo [b], Alberto Ceccon [a,*]

[a] Dipartimento di Scienze Chimiche, Università degli Studi di Padova, via Marzolo 1, 35131 Padova, Italy
[b] CNR, Istituto di Chimica Inorganica e delle Superfici, C.so Stati Uniti 4, 35127 Padova, Italy

ARTICLE INFO

Article history:
Received 1 August 2008
Received in revised form 3 September 2008
Accepted 22 September 2008
Available online 27 September 2008

Dedicated to Professor Christopher Elschenbroich on the occasion of his 70th birthday

Keywords:
Heterobimetallic
Mixed valence
Ferrocenyl
Chromium-tricarbonyl
Electron transfer

ABSTRACT

A series of heterobimetallic η^6-[(ferrocenyl)indene]-$Cr(CO)_3$ complexes differing for the position of the ferrocenyl group, 1-(ferrocenyl)indene and 2-(ferrocenyl)indene, and the degree of indene methylation (tetramethyl- and hexamethyl-) have been prepared and studied with the aim to stabilise the mono- and dications generated by chemical and electrochemical oxidation, and at same time to tune the metal–metal electronic coupling in the mixed-valence cations. The magnitude of electronic delocalisation and spin density in the cations have been monitored by means of optical techniques (UV–Vis, near-IR, mid-IR) and EPR spectroscopy. The results have been rationalised in the framework of Marcus-Hush theory and at quantum chemistry level by DFT and TD-DFT methods, establishing that a metal-to-metal electronic coupling occurs the magnitude of which depends on the degree of indene methylation.

1. Introduction

Electronic communication in polynuclear complexes has received, and currently receives, a great interest with special regard to bimetallic complexes in which the two metals are linked by a π-electron conjugated system [1]. In particular, much attention has been paid to those systems in which two transition metal groups, ML_n, are bound to a fulvalenyl bridge [2]. Depending on the flexibility of the bridge and the nature of the metal groups the degree of coupling may vary to a large extent. In this regard, while complexes featuring two equivalent redox centres as ferrocene ($M_1 = M_2$; symmetric complexes) represent the most investigated class, complexes with two different metals ($M_1 \neq M_2$; unsymmetrical complexes) have received much less attention likely because of their synthetic difficulty.

Despite some important results on the communication in heterobimetallic complexes that have been obtained in recent years [3], the effect of the "metal asymmetry factor" in determining the extent of the communication is still little known.

In a preliminary communication [4], we have reported on the structures and the electrochemical behaviour of two heterobimetallic isomers, η^6-(3-ferrocenyl)indene]-$Cr(CO)_3$ (**1**) and η^6-(2-ferrocenyl)indene]-$Cr(CO)_3$ (**2**). By combining these results with the IR and near-IR data on the mixed-valence ions $\mathbf{1}^+$ and $\mathbf{2}^+$ obtained at −80 °C by chemical oxidation with ferrocenium-BF_4 in CH_2Cl_2, it was shown that electronic coupling is principally in $\mathbf{2}^+$ and much less in $\mathbf{1}^+$. The stronger electronic coupling in $\mathbf{2}^+$ was attributed to the almost planarity of the bridging ligand and to the *cisoid* conformation of the two metal groups. The planarity of the two cyclopentadienyl-indene (Cp-indene) moieties favours the π-electron resonance in the corresponding conjugated atom grouping of the bridge. In contrast, in isomer **1** the metals exhibit a *transoid* arrangement and the bridge shows a torsion angle about the σ-bond of around 30°.

Described in this contribution is a complete study of the electronic interaction occurring between the iron and chromium centres in the (ferrocenyl)indenyl complexes shown in Scheme 1.

The information gathered by EPR, near-IR spectroscopy, and DFT calculations indicate that the cations of the parent complexes **1** and **2** and of the methylated complexes η^6-[(3-ferrocenyl) 1,2,4,5,6,7-hexamethylindene]-$Cr(CO)_3$ (**3**), η^6-[(2-ferrocenyl) 4, 5,6,7-tetramethylindene]-$Cr(CO)_3$ (**4**), and η^6-[(2-ferrocenyl) 1,3,4,5,6,7-hexamethylindene]-$Cr(CO)_3$ (**5**) (Scheme 1) belong to the mixed-valence Class II according to the classification of Robin and Day and that the extent of the metal-metal electronic interaction can be modulated by the degree of methylation and cyclopentadienyl-indene planarity. Accordingly, the results of the

* Corresponding authors.
E-mail address: saverio.santi@unipd.it (S. Santi).

0022-328X/$ - see front matter © 2008 Elsevier B.V. All rights reserved.
doi:10.1016/j.jorganchem.2008.09.024

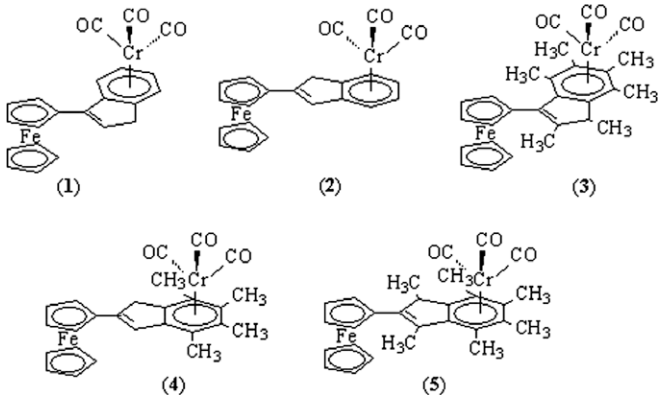

Scheme 1.

CO-substitution-P(OEt_3)-addition reaction of $\mathbf{1}^+$ and $\mathbf{2}^+$ are in favour of an activation of chromium mediated by an oxidative process at the iron atom.

The methylation of the indenyl skeleton, as expected, stabilises both mono and dications due to the electronic and steric effects of the methyl groups and modifies the planarity of the bridge to some extent.

2. Results and discussion

2.1. Synthesis and structures

The synthetic procedure of heterobimetallic complexes **1** and **2** [4] was successfully applied to **3**–**5** starting from the corresponding monometallic (ferrocenyl)indenes [5]. The crystal structures of **3** and **5** have been obtained and compared with those of **1** and **2** previously reported [4] (Fig. 1, Tables 1 and 2). In this regard, we could justify the *transoid* conformation of **1** (Fig. 1a) and the *cisoid* conformation of **2** (Fig. 1b) in terms of co-existence of balanced weak intramolecular π-hydrogen bond interactions and competitive van der Waals repulsive interactions, suggesting that *transoid* or *cisoid* conformations are expected to be almost isoenergetic for both **1** and **2**. The molecular structure of **3** (Fig. 1c, Table 1) supports this hypothesis at least for the case of complex **1**. In Table 2 some geometrical parameters are reported.

Actually, in **3** the ferrocenyl group is bonded in a *cisoid* orientation, in contrast with the *transoid* conformation of **1**, giving rise to a π-hydrogen bond interaction between H12 and the carbonyl C1=O1 at the distance H12…O1 of 2.84 Å. The $Cr(CO)_3$ group assumes a staggered *endo*-conformation. The observed molecular conformation is tolerated in spite of the presence of the bulky methyl groups which produce quite short and strongly repulsive intramolecular non-bonded carbon–carbon contact distances in the range of 3.00 Å (see C28…C5 = 3.04 Å), typical of an overcrowded molecular structure.

It is to be noted that in the case of **1** an analogous *cisoid* conformation would produce the same π-hydrogen bond interaction and a very short contact between H5 and H19 at a distance of ca. 2.00 Å, as it can be verified by exchanging the methyl group C28 with a H atom in **3**.

The torsion angle about the bond C4–C14 joining the ferrocenyl group to the indene ligand is here around 45° similar to that in **1,** so excluding any relevant resonance effect in the Cp-indene. These results lead to surmise that for **1** a similar *cisoid* conformation would be reasonably predictable, although probably a little less stable. A *cisoid* orientation of $Cr(CO)_3$ with respect to the methyl group C24 is clearly disfavoured for steric reasons; this fact is not present in the case of the corresponding non-methylated complex in the absence of the stereoisomeric centre on C16.

Interestingly, in the reaction conditions complex **3** undergoes a 1–3 (H16–H14) *protonic shift* giving rise to the isomeric molecular structure **3′** (Fig. 1e) in which very short intramolecular C…C contact interactions are absent, thus favouring a decreasing of its internal conformational energy. We think that this *protonic shift* is promoted by the necessity to relieve the molecular constraints present in the isomeric complex **3**. We note that in the case of the complex **1**, where similar constraints are absent, this *protonic shift* has not been observed. All the carbon-carbon non-bonded distances are larger than 3.20–3.25 Å. The ferrocenyl group is *transoid* with respect to $Cr(CO)_3$, which assumes here too a staggered *endo*-conformation. The less common *endo-staggered* [5] conformations of the $Cr(CO)_3$ groups, observed both in **3** and in **3′** in contrast with the *exo-staggered* [5] conformation of **1,** are likely someway influenced by the vicinal methyl groups which form a number of probable weak π-hydrogen bond interactions in the range of ca. 2.8–2.9 Å. Here too, the configuration having the $Cr(CO)_3$ group *cisoid* with respect to the ferrocenyl group appears to be more disfavoured for steric reasons.

The molecular structure of **5** is shown in Fig. 1f and its geometrical parameters are reported in Table 2. The conformation of the (2-Cp)-hexamethylindene skeleton is almost the same as that of the monometallic (2-ferrocenyl)hexamethylindene [6]. The torsion angle C1–C2–C11–C12 is around 23°, as compared with 24–25° there observed, proving that the conformation is still controlled by the repulsive interactions between H3…H15 and H1…C24 at distances of 2.31 and 2.88 Å, respectively. The $Cr(CO)_3$ group assumes an eclipsed conformation which allows probable π-hydrogen bonding interactions between O3…H10 and O3…H15 at distances of 2.85 and 2.79 Å, respectively.

2.2. Electrochemistry

The electrochemical oxidation within cyclic voltammetry (CV) experiments of the bimetallic complexes **1**–**5** (Fe^{II}–Cr^0) into their cationic and dicationic forms displays two fully reversible waves (Fig. 2) occurring at E_p in the range of 0.51–0.59 (Fe^{III}–Cr^0) and 0.72–0.89 (Fe^{III}–Cr^I) V versus SCE in CH_2Cl_2/0.1 M n-Bu_4NPF_6 (Table 3).

The $\Delta E_{1/2}$ values which are indicative of thermodynamic stability of the cationic species with respect to disproportionation [7] and the related values of the equilibrium constant (Table 3) for the comproportionation, K_c (Eq. (1)), suggest that is possible to characterise the mixed-valence cations $\mathbf{1}^+$–$\mathbf{5}^+$ in solution.

$$[Fe^{II} - Cr^0] + [Fe^{III} - Cr^I] = 2[Fe^{III} - Cr^0] \quad (1)$$

Interestingly, the peak separation of the two waves in **1**–**5** in the range of 210–300 mV is almost the same found between the monometallic compounds, i.e. ferrocene and (indene)$Cr(CO)_3$ (**6**) or (heptamethylindene)$Cr(CO)_3$ (**7**) (Table 3). As the CVs of the bimetallic complexes are approximately the sum of the CVs of monometallic compounds, it might appear that communication at the level of $\mathbf{1}^+$–$\mathbf{5}^+$ is almost absent. In contrast, chemical and optical data will show that electronic communication between iron and chromium exists (*vide infra*).

2.3. The addition-substitution reaction of $\mathbf{1}^+$ and $\mathbf{2}^+$ with $P(OEt)_3$

It was determined [8] that the oxidation of benzene-$Cr(CO)_3$ in the presence of $P(OEt)_3$ leads to rapid substitution of one CO according to Scheme 2

$$(Ar)Cr(CO)_3 \overset{-e^-}{\rightleftharpoons} (Ar)Cr(CO)_3^+ \xrightarrow[-CO]{P(OEt)_3} (Ar)Cr(CO)_2P(OEt)_3^+ \overset{+e^-}{\rightleftharpoons} (Ar)Cr(CO)_2P(OEt)_3$$

Scheme 2.

In addition, in $(C_6H_5Fc)Cr(CO)_3$ the Fc group acts as a reversible redox switch and activates the oxidative ligand substitution and addition reactions at the chromium. In this case, the potential required for activation is far lower than otherwise needed. The small shift of the IR carbonyl stretching energies of the $Cr(CO)_3$ group upon oxidation demonstrate that in $[(C_6H_5Fc)Cr(CO)_3]^+$ the positive charge is localised at the iron. However, the chromium centre acquires sufficient radical character and undergoes very rapid CO

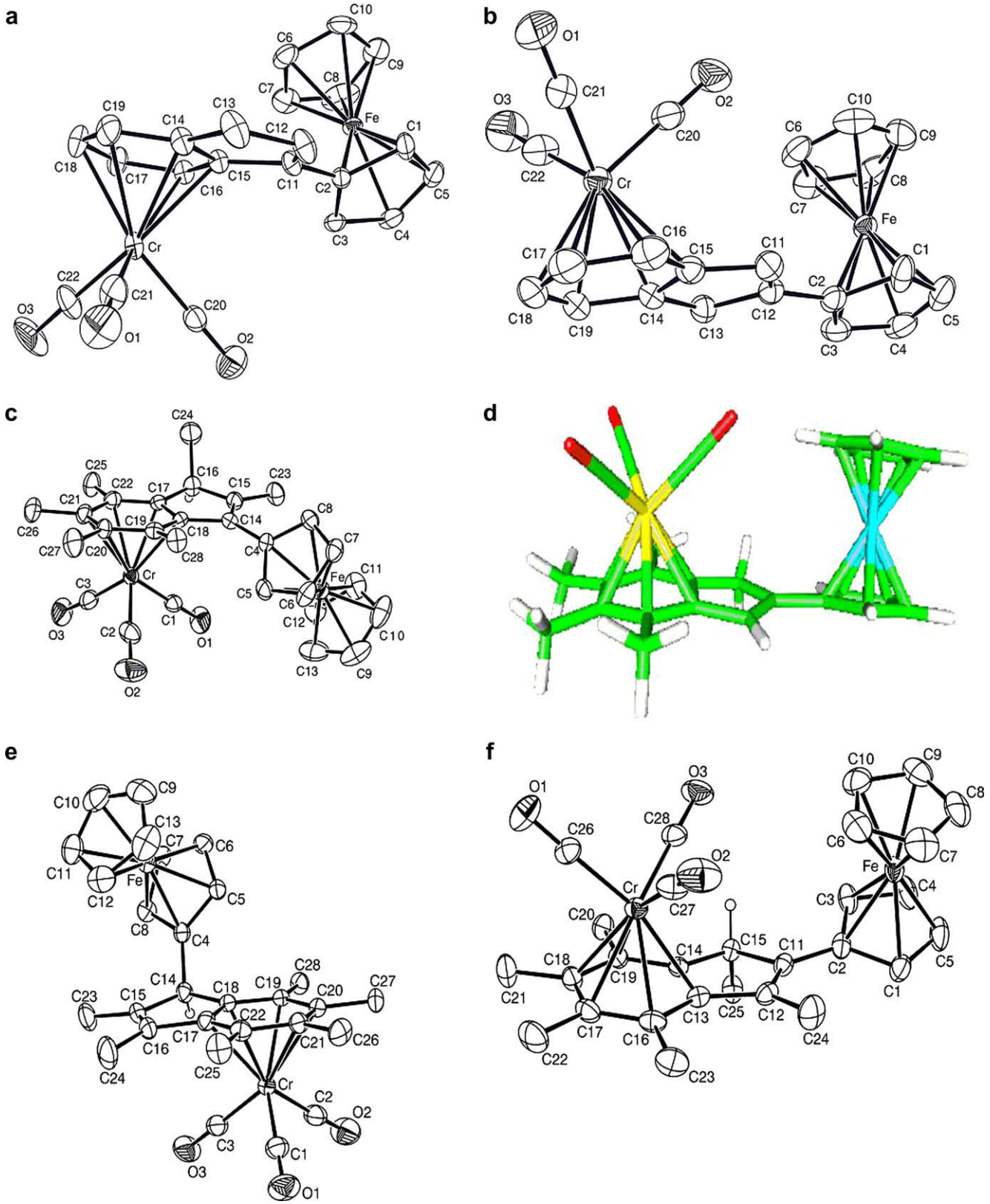

Fig. 1. Molecular structures of (a) **1**, (b) **2**, (c) **3**, (e) **3′**, (f) **5,** and (d) DFT calculated structure of **4**. In the ORTEP plots hydrogen atoms have been omitted for clarity.

Table 1
Crystallographic data for complexes **3** (c), **3′**(d), **5** (f)

Compound	**3 (c)**	**3′ (e)**	**5 (f)**
Empirical formula	$C_{28}H_{28}O_3CrFe$	$C_{28}H_{28}O_3CrFe$	$C_{28}H_{28}O_3CrFe$
M	520.35	520.35	520.35
Crystal system	Orthorhombic	Triclinic	Monoclinic
Space group	$P2_12_12_1$	$P\bar{1}$	$P21/c$
a (Å)	13.540(2)	7.957(2)	10.523(2)
b (Å)	14.476(3)	9.829(3)	13.455(3)
c (Å)	12.298(3)	16.496(3)	16.648(3)
α (°)	–	105.65(3)	–
ß (°)	–	90.05(2)	91.02(3)
γ (°)	–	106.14(2)	–
V (A^3)	2410.5(8)	1189.3(5)	2356.8(8)
Z	4	2	4
$D_{calcd.}$ (g cm^{-3})	1.434	1.641	1.467
μ (Mo Kα) (mm^{-1})	0.741	0.725	1.104
F(000)	1080	2688	1080
No. of reflections collected	2786	3941	5462
No. of reflections used [$I \geqslant 2\sigma(I)$]	2461	3775	5181
Goodness-of-fit on F^2	1.186	1.208	1.236
$R = \sum\|F_o\| - \|F_c\|/\sum\|F_o\|$	0.048	0.043	0.060
$Rw = \{\sum[w(F_o^2 - F_c^2)^2]/\sum[w(F_o^2)^2]\}^{1/2}$	0.103	0.110	0.171

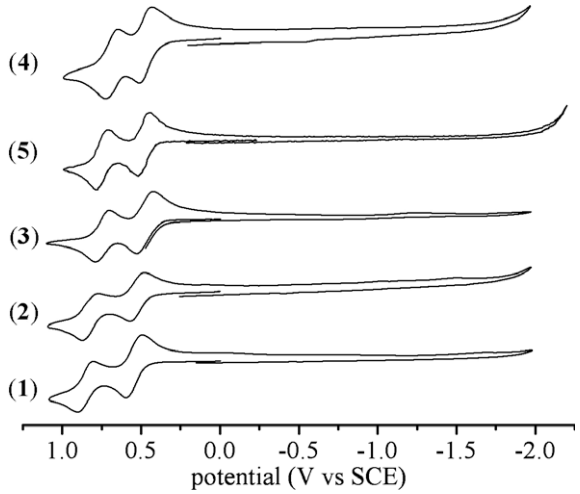

Fig. 2. CVs of complexes **1**-**5** in CH_2Cl_2/0.1 M *n*-Bu_4NPF_6 at scan rate *v*; = 0.5 V s^{-1}.

substitution by $P(OEt)_3$. Concomitant internal electron transfer from chromium-to-iron occurs with the result that the ferrocenium group in $[(C_6H_5Fc)Cr(CO)_2P(OEt)_3]^+$ reverts to ferrocenyl. Further oxidation of Fc leads to the addition of a second phosphite and formation of $[(C_6H_5Fc)Cr(CO)_2(P(OEt)_3)_2]^{2+}$ [8].

For comparison, we carried out the electrochemical oxidation of the monometallic $Cr(CO)_3$ complexes **6** and **7** in the presence of $P(OEt)_3$, and of the heterobimetallic complexes **1** and **2** in which the (benzene)$Cr(CO)_3$ and the Fc moieties are not directly connected but spanned by a cyclopentadiene linkage. Complexes **6** and **7** leads to rapid substitution of one CO according to Scheme 2 and the electrochemical behaviour is shown in Fig. 3.

In the presence of 0.5 equivalent of nucleophile, the CV of **6** (Fig. 3b) shows a splitting of the initial oxidation wave which is ab-

Table 3
Electrochemial data[a]

Complex	E_p (V)		$E_{1/2}$ (V)		$\Delta E_{1/2}$ [b] (V)	K_c
	Fe	Cr	Fe	Cr		
1	0.591	0.899	0.556	0.865	0.309	2.1×10^5
2	0.566	0.869	0.532	0.835	0.303	1.6×10^5
3	0.525	0.788	0.486	0.757	0.271	4.6×10^4
4	0.510	0.720	0.475	0.691	0.216	5.2×10^3
5	0.516	0.781	0.487	0.751	0.264	3.5×10^4
Fc	0.512	–	0.480	–	–	–
6	–	0.810	–	0.760	–	–
7	–	0.640	–	0.608	–	–

[a] Solvent was CH_2Cl_2, supporting electrolyte 0.1 M *n*-Bu_4NPF_6, scan rate 0.5 V s^{-1}. All potentials are in Volts vs. SCE.
[b] $\Delta E_{1/2} = E_{1/2}(Cr) - E_{1/2}(Fe)$.

Table 2
Selected interatomic distances (Å) and angles (°) of complexes $\mathbf{1}^{0/+}$, $\mathbf{2}^{0/+/2+}$, $\mathbf{3}^{0/+}$, **3′**, $\mathbf{4}^{0/+/2+}$ and $\mathbf{5}^{0/+/2+}$;[a] relative energies (E_{rel}, eV) and adiabatic ionization potentials (IP, eV)

	Fe—Q_1[b]	Fe—Q_2[b]	Fe–Cr	Cr—Q[c]	Cr–CO[d]	C2–C11[e]	Δ1[f]	Δ2[f]	E_{rel}	IP
1[g]	1.667	1.661	5.913	1.755	1.838	1.464	−28	−32		
	1.653(8)	*1.635(9)*	*5.777(2)*	*1.747(8)*	*1.821(6)*	*1.464(6)*	*−31.8(7)*	*−34.3(4)*		
$\mathbf{1}^+$	1.704	1.709	5.951	1.762	1.859	1.465	−30	−29		6.508
2[g]	1.671	1.658	6.404	1.761	1.83	1.451	−12	−10		
	1.642(6)	*1.641(8)*	*6.269(2)*	*1.744(6)*	*1.827(5)*	*1.461(6)*	*−10.2(7)*	*−6.1(7)*		
$\mathbf{2}^+$	1.702	1.710	6.419	1.770	1.857	1.447	−12	−6		6.370
$\mathbf{2}^{2+}$(**T**)	1.747	1.739	6.599	1.808	1.889	1.457	−13	−6		10.124
3	1.663	1.668	5.739	1.767	1.831	1.481	48.1	40.9		
	1.648(7)	*1.651(8)*	*5.639(2)*	*1.744(7)*	*1.816(8)*	1.459(8)	*50.1(9)*	*41.2(9)*		
3′	1.665	1.669	6.408	1.760	1.835	1.536	−65.1	5.9		
	1.649(7)	*1.653(7)*	*6.227(2)*	*1.734(6)*	*1.824(4)*	*1.522(6)*	−6.19(6)	*8.4(6)*		
$\mathbf{3}^+$	1.703	1.707	5.721	1.784	1.851	1.475	45.2	41.8		6.140
4	1.657	1.670	6.458	1.771	1.834	1.451	−13	−9		
$\mathbf{4}^+$	1.696	1.705	6.419	1.784	1.853	1.445	−14	−8		4.574
$\mathbf{4}^{2+}$(**T**)	1.743	1.738	6.601	1.818	1.880	1.455	−10	−6	+0.001	9.475
$\mathbf{4}^{2+}$(**S**)	1.742	1.739	6.583	1.816	1.882	1.455	−13	−8	0	9.474
5	1.656	1.670	6.413	1.769	1.833	1.462	−13.2	−8.8	–	
	1.642*(4)*	1.640*(4)*	5.886*(2)*	*1.726(3)*	*1.830(4)*	*1.462*	−22.9(6)	*−21.0(4)*		
$\mathbf{5}^+$	1.697	1.707	6.354	1.776	1.850	1.452	−15.4	−6.3		6.049
$\mathbf{5}^{2+}$(**T**)	1.741	1.738	6.443	1.813	1.879	1.460	−15.6	−7.2	+0.005	9.438
$\mathbf{5}^{2+}$(**S**)	1.738	1.737	6.447	1.811	1.880	1.459	−15.6	−7.0	0	9.433

[a] Crystallographic data are reported in italics.
[b] $Q_{1,2}$ denotes the centroid of the Cp rings of the ferrocenyl unit.
[c] Q is the center of the benzene moiety of the indenyl ring.
[d] Average distance.
[e] For **3** and **3′** the C4–C14 and for **2** the C2–C12 bonds are reported.
[f] Dihedral angle describing the torsion about the C2–C11 bond.
[g] From Ref. [4].

sent in the CV of **7** (Fig. 3e). This occurs because there is a deficiency of phosphite and the second-order reaction of the cation with $P(OEt)_3$ is very rapid and faster for $\mathbf{6}^+$ than for $\mathbf{7}^+$. By addition of one equivalent of $P(OEt)_3$ the initial oxidation wave becomes chemically irreversible (Fig. 3c and f). The reversible wave appearing in the cathodic scan reversal corresponds to the redox couples [(indene)$Cr(CO)_2P(OEt)_3$] (**6P**/**6P**$^+$) (0.27 V) and [(heptamethylindene)$Cr(CO)_2P(OEt)_3$] (**7P**/**7P**$^+$) (0.05 V). Due to the instability of the non-methylated **6P**$^+$ only the formation of **7P**$^+$ was monitored by IR (Fig. 4).

Oxidation of **7** ($\tilde{\nu}_{CO}$) = 2049, 1976–1946 cm^{-1}) with equimolar oxidising agent acetylferrocenium[BF_4] shows a positive shift of the carbonyl bands ($\tilde{\nu}_{CO}$) by around 110 cm^{-1} indicating that a positive charge is localised at chromium in **7**$^+$ (Fig. 4b). Oxidation in the presence of one equivalent of $P(OEt)_3$ results in the formation of the purple species **7P**$^+$ with $\tilde{\nu}_{CO}$ at 1972 and 1886 cm^{-1} (Fig. 4c). Addition of a second equivalent of $P(OEt)_3$ and oxidising agent leads to the formation of the diphosphite dication [(heptamethylindene)$Cr(CO)_2P(OEt)_3]^{2+}$ (**7P**$_2^{2+}$) (Fig. 4d) which was isolated and characterised.

Our purpose was to determine if the chromium site in the cations of η^6-[(ferrocenyl)indene]-$Cr(CO)_3$ complexes is activated to CO substitution even though the iron and not the chromium centre is oxidised.

The IR spectra of the cations **1**$^+$**–5**$^+$ obtained by stepwise oxidation in the range of 0.0–0.6 V of the neutral compounds in an OTTLE spectroelectrochemical cell display almost complete reversibility ($\geqslant$95%) upon cathodic scan reversal. At −45 °C all the cations **1**$^+$–**5**$^+$ display small positive shifts (4–11 cm^{-1}) of the carbonyl stretching bands indicating that the positive charge is almost localised at the iron centre. By increasing the potential up to the second oxidation wave two new bands appear in the IR spectrum of **1**$^+$, **3**$^+$, **4**$^+$ and **5**$^+$ shifted at higher wavenumbers by around 120 cm^{-1} characteristic of the corresponding dicationic species (Table 4).

The oxidation of **1** and **2** with and without $P(OEt)_3$ was monitored by CV and IR and the results for **2** are shown in Fig. 5. It appears from the comparison of Fig. 5a and b that **2**$^+$ reacts rapidly with $P(OEt)_3$. The main features are (i) partial loss of chemical reversibility of the first oxidation wave; (ii) a new reversible oxidation wave at E_p = 0.72 V; (iii) a reversible wave at around 0.2 V; (iv) a chemically irreversible reduction wave at E_p = 0.26 V. The CVs of Fig. 5b suggest the existence of a mechanism (Scheme 3) analogous to that previously proposed by Sweigart [8] in which $P(OEt)_3$ attacks the chromium centre in **2**$^+$ and the stable complex [η^6-(2-ferrocenyl)indene]-$Cr(CO)_2[P(OEt)_3]_2^{2+}$ (**2P**$_2^{2+}$) is formed.

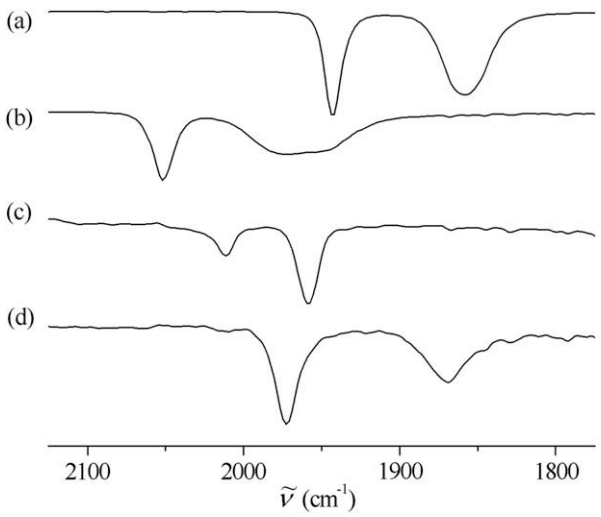

Fig. 4. IR spectra in CH_2Cl_2 of (a) **7**, (b) **7**$^+$, (c) **7P**$^+$ and (d) **7P**$_2^{2+}$. T = 20 °C.

Table 4
IR bands in the carbonyl region in CH_2Cl_2

	$\tilde{\nu}_{CO}$ (cm^{-1})	
1	1956	1875
1$^+$	1961	1884
1^{2+}	2070	1997
2	1954	1873
2$^+$	1960	1887
3	1940	1854
3$^+$	1944	1862
3^{2+}	2053	1980
5	1939	1857
5$^+$	1943	1868
5^{2+}	2058	1989
6	1954	1871
6$^+$	2067	2000–1979
7	1938	1852
7$^+$	2049	1976–1946

The preparation of an authentic sample of **2P**$_2^{2+}$ was achieved by chemical oxidation of **2** (1954 and 1873 cm^{-1}) by addition of two equivalents of acetylferrocenium[BF_4] in the presence of two equivalents of $P(OEt)_3$. The purple complex was easily isolated

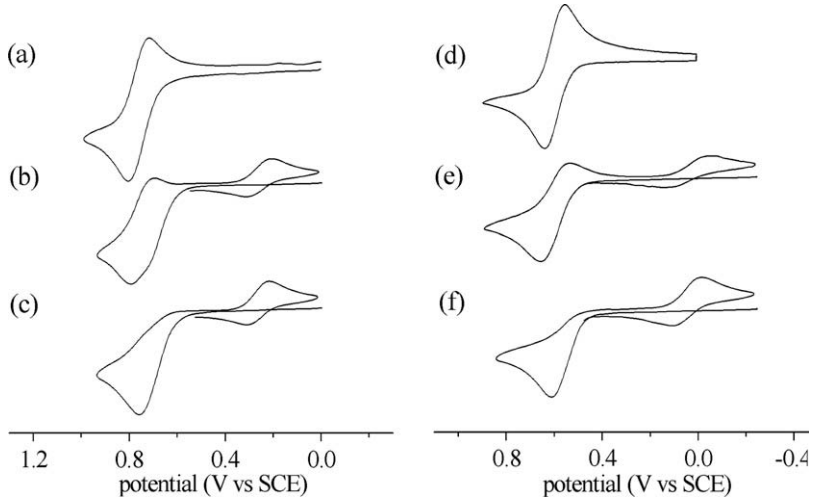

Fig. 3. CVs in CH_2Cl_2/0.1 M n-Bu_4NPF_6 at scan rate v; = 0.5 V $s^{-1}$of 3 mM (a) **6** and (d) **7** in the presence (b,e) 0.5 and (c,f) 1 equiv. of $P(OEt)_3$.

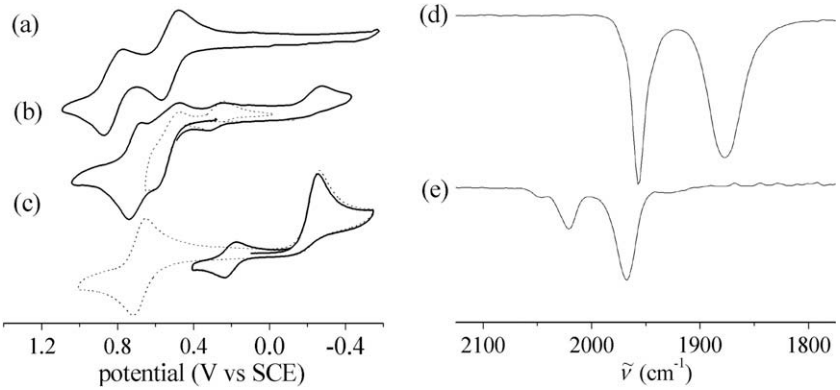

Fig. 5. Reactivity of $\mathbf{2}^{+}$ with $P(OEt)_3$. Cyclic Voltammetry in CH_2Cl_2/0.1 M n-Bu_4NPF_6 at scan rate v; = 0.5 V s^{-1} of (a) 3 mM **2**; (b) **2** in the presence of 2 equiv, of $P(OEt)_3$; (c) anodic (dotted line) and cathodic scan (dashed line) of $\mathbf{2P_2^{2+}}$. IR spectra in in CH_2Cl_2 of (d) **2** and (e) $\mathbf{2P_2^{2+}}$.

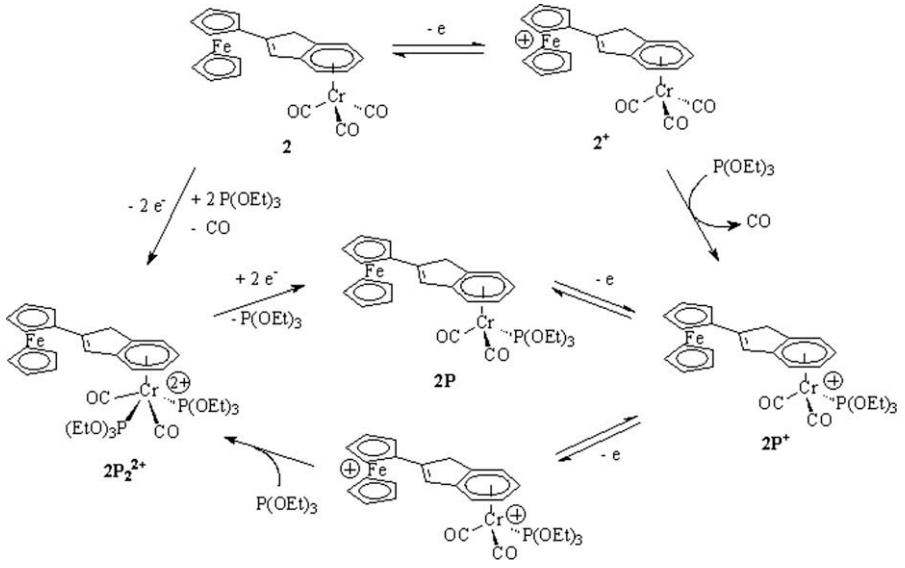

Scheme 3.

and characterised as the BF_4 salt and its ^1H and ^{31}P NMR spectra are consistent with the proposed structure. The isolated purple species shows two $\tilde{\nu}_{CO}$ bands at 2020 and 1968 cm^{-1} (Fig. 5d and e) similar to those of $\mathbf{7P_2^{2+}}$.

The relative intensities of the IR bands of $\mathbf{2P_2^{2+}}$ imply a *trans* rather than *cis* arrangement of the COs [8]. It appears that all the new oxidation and reduction waves present in the CV of Fig. 5b match to those of Fig 5c. The CV of $\mathbf{2P_2^{2+}}$ (Fig 5c) shows reversible oxidation of the ferrocenyl at E_p = 0.72 V. The reduction of $\mathbf{2P_2^{2+}}$ occurs irreversibly (E_p = 0.26 V) and the reversible wave at $E_{1/2}$ = 0.20 V after scan reversal is assigned to the redox couple $\mathbf{2P/2P^{+}}$. The conclusion is that reduction of $\mathbf{2P_2^{2+}}$ is a 2-electron process, generating **2P** and free $P(OEt)_3$. Similar electrochemical and IR results have been obtained for **3** and the corresponding dication $\mathbf{3P_2^{2+}}$ has been isolated and characterised, too. In particular, the reduction of $\mathbf{3P_2^{2+}}$ lead to the appearance of the reversible redox couple $\mathbf{3P/3P^{+}}$ at 0.28 V. The comparison of the $E_{1/2}$ values found for $\mathbf{6P/6P^{+}}$, $\mathbf{2P/2P^{+}}$ and $\mathbf{3P/3P^{+}}$ (0.26, 0.28 and 0.20 V, respectively) allows the evaluation of the ferrocenyl substituent effect on the oxidation potential of the chromium site. This substituent effect, $\Delta E'$, can be reasonably approximated as 60 mV when the ferrocenyl is in 2-position, and almost null in 3-position.

2.4. EPR spectroscopy

EPR spectra of monocations of monometallic $\mathbf{6^{+}}$, $\mathbf{7^{+}}$ and [(3-ferrocenyl)hexamethylindene]$^{+}$ ($\mathbf{8^{+}}$), and bimetallic complexes $\mathbf{1^{+}}$, $\mathbf{2^{+}}$ $\mathbf{3^{+}}$ and $\mathbf{5^{+}}$, prepared by chemical oxidation, were obtained in frozen solution at cryogenic temperatures. Details of the oxidation procedure are reported in the Section 4. Fig. 6 shows the EPR spectrum of $\mathbf{7^{+}}$ in CH_2Cl_2 glass at 10 K. A similar spectrum has been obtained for the corresponding non-methylated complex $\mathbf{6^{+}}$ (data not shown). They exhibit a nearly axial powder spectrum, characterised by unresolved features for the different components of the g-matrix. The main component is larger (g = 2.04) than the free-electron value, as expected for a mononuclear Cr(I) species with a strong metallic character in the single occupied molecular orbital [9–11].

Fig. 7 compares the EPR spectra of $\mathbf{8^{+}}$ with the corresponding dinuclear complex $\mathbf{3^{+}}$ in CH_2Cl_2 glass at 10 K, where no major difference can be observed. The EPR spectra of both complexes are characterised by a large g-anisotropy (Δg = 1.9) and concomitant rapid spin-lattice relaxation behaviour, which did not allow signal detection above liquid helium temperatures. These magnetic properties are typical of low-spin Fe(III) systems and have been reported also for ferrocenium ions [12,13]. Similar results have been obtained when comparing the heterobimetallic cations $\mathbf{1^{+}}$,

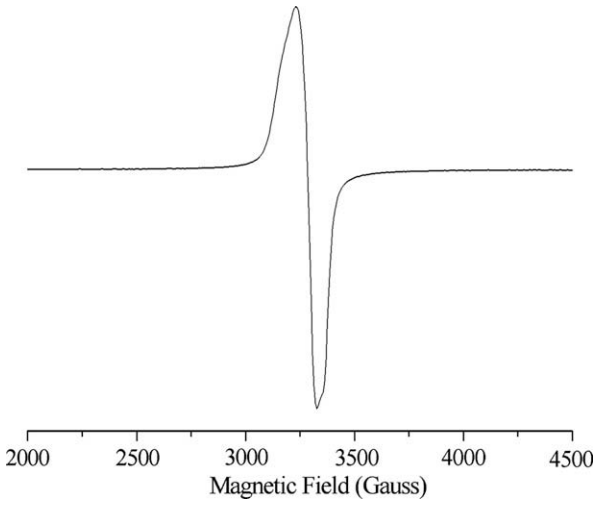

Fig. 6. X-band EPR spectrum of [(heptamethylindene)Cr(CO)$_3$] (**7**$^+$) (2 mM) in CH_2Cl_2 glass at 10 K. Parameters are given in the experimental section.

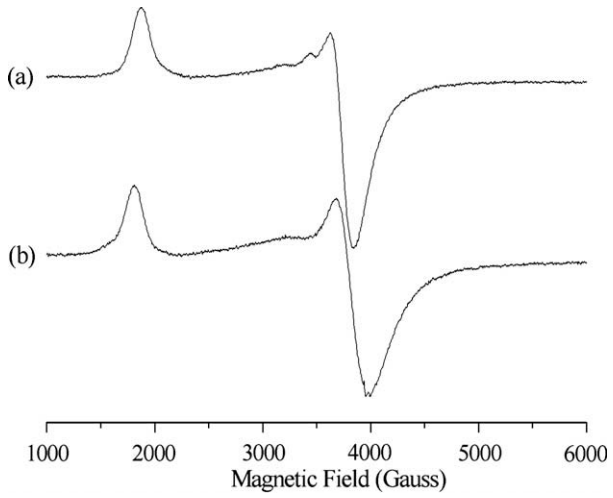

Fig. 7. X-band EPR spectra of [(3-ferrocenyl)hexamethylindene]$^+$ (a) and corresponding bimetallic complex **3**$^+$ (b) in CH_2Cl_2 glass (2 mM) at 10 K. Parameters are given in Section 4.

2$^+$and **5**$^+$, with the corresponding monometallic cations **8**$^+$ and [(2-ferrocenyl)hexamethylindene]$^+$ (**9**$^+$): no reduction in the degree of *g*-factor anisotropy has been observed in the dinuclear species at cryogenic temperatures.

The value of Δg can be used to classify mixed-valence complexes in terms of the rate of electron transfer between the metal sites in the EPR time-scale [13]. The high degree of *g*-anisotropy of the monometallic and bimetallic cations, is diagnostic of electronic localisation in the mixed-valence cations in the EPR time-scale.

Furthermore, from helium temperatures up to 150 K no contribution of the Cr(I) moiety to the EPR spectra of the heterobimetallic **1**$^+$, **2**$^+$ **3**$^+$and **5**$^+$ has been found while the corresponding Cr(I) signal in the monometallic complexes (**6**$^+$ and **7**$^+$) has been detected up to 150 K. The detrapping phenomenon, which would lead to a reduction of the *g*-anisotropy of the EPR spectrum of the ferrocenium moiety and concomitant appearance of the signal due the presence of Cr(I), could not be verified at temperatures higher than 150 K because of the presence of traces of decomposition above the melting point of the solvent.

When considering whether there is delocalization between two metal centers, the time-scale of the spectroscopic technique is an important issue. We have verified that in the EPR time-scale, which is longer than the optical spectroscopy time-scale, detrapping in the heterobimetallic complexes does not occur at least at cryogenic temperatures, suggesting electron transfer rates much slower than 10^8 s^{-1}. Localized mixed-valent behaviour in frozen glass and occurrence of delocalization only at higher temperatures or in fluid solution was reported for both diferrocenyl and dichromium monocation complexes [13–15].

2.5. Near-IR spectroscopy

The near-IR is a spectral region diagnostic for donor-acceptor charge transfer processes [16]. Measurements on **1**$^+$–**5**$^+$ obtained in CH_2Cl_2 by spectroelectrochemistry at −45 °C and by chemical oxidation with ferrocenium[BF_4] at −80 °C revealed the appearance of a new band in the range 6000–10 000 cm^{-1}, the intensity and energy of which depend on the position of the ferrocenyl group and on the methylation of the indene moiety. The effect of

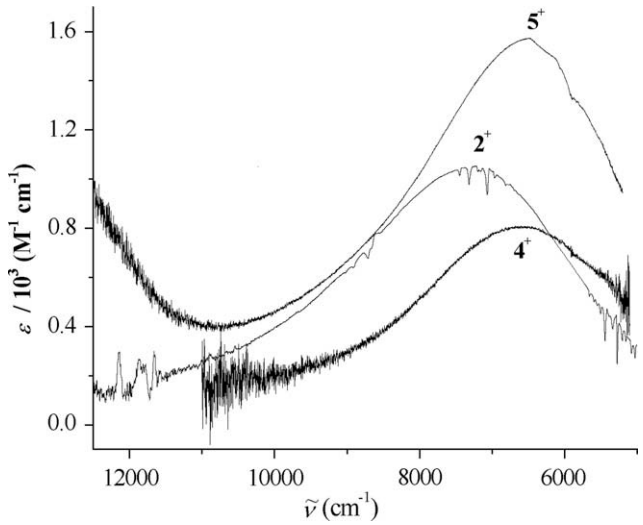

Fig. 8. Near-IR spectra of 3.0 mM **2**$^+$, **4**$^+$ and **5**$^+$ in CH_2Cl_2.

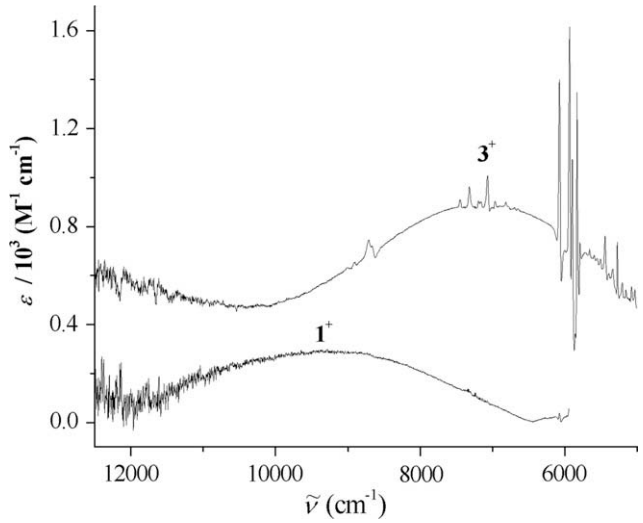

Fig. 9. Near-IR spectra of 3.0 mM **1**$^+$ and **3**$^+$ in CH_2Cl_2.

Table 5
Near-IR Data in CH_2Cl_2/*n*-Bu_4NPF_6

	$\tilde{\nu}_{max}$[a] (cm^{-1})	E_0 (cm^{-1})	ε_{max} [mol cm^{-3} cm^{-1}]	$(\Delta\tilde{\nu}_{1/2})_{obsd}$ (cm^{-1})	$(\Delta\tilde{\nu}_{1/2})_{calcd}$ (cm^{-1})	H_{ab} (cm^{-1})	α	$\Delta G^{\neq}$ (kJ mol^{-1})
1$^+$ [b]	9355	1775	289	3029	3359	328	0.035	30.8 (30.7[c])
2$^+$ [b]	7480	1451	960	3080	2996	468	0.063	22.7 (22.5[c])
3$^+$ [c]	7059	887	872	3104	3295	510	0.072	18.6
4$^+$ [c]	6600	564	630[d]	3021	3258	372	0.056	17.4
5$^+$ [c]	6626	448	1571	3207	3296	598	0.090	14.8

[a] ±4 cm^{-1}.
[b] $T = -80$ °C.
[c] $T = -45$ °C.
[d] The cation **4**$^+$ decomposes during the acquisition.

both methylation of indene and position of ferrocene is evidenced in Figs. 8 and 9.

In particular, the intensity of the band in the "linear" 2-isomers **2**$^+$, **4**$^+$ and **5**$^+$ is higher than in the "non linear" 3-isomers **1**$^+$ and **3**$^+$ (Table 5).

A powerful probe for evaluating the magnitude of the metal–metal interaction in mixed-valence compounds is represented by the analysis of the IT bands in the near-IR region by using the classical two-state electron transfer model (Hush theory) [17].

According to Robin and Day classification [16b], three classes of mixed-valence systems can be distinguished on the basis of the magnitude of metal–metal electronic coupling. The strength of electronic interaction between the oxidised and reduced sites ranges from essentially zero (Class I) to moderate (Class II), to very strong electronic coupling (Class III). In the case of Class II regime $\Delta\tilde{\nu}_{1/2}$ can be calculated by using Hush Eqs. (2) and (3)

$$(\Delta\tilde{\nu}_{1/2})_{Hush}\ (cm^{-1}) = [16RT\ln 2(\tilde{\nu}_{max}E_0)]^{1/2} \quad (2)$$

The experimental half-bandwidth, $(\Delta\tilde{\nu}_{1/2})_{obsd}$ and that calculated by using Hush Eqs. (2) and (6), $(\Delta\tilde{\nu}_{1/2})_{calcd}$, are quite similar as expected for a Class II mixed-valence species. In this regime, the electronic coupling H_{ab} is given by Eq. (3) [16,17]

$$H_{ab} = \frac{0.0205(\varepsilon_{max}\tilde{\nu}_{max}\Delta\tilde{\nu}_{1/2})^{1/2}}{d} \quad (3)$$

$$\alpha = \frac{H_{ab}}{\tilde{\nu}_{max}} \quad (4)$$

in which d represents the adiabatic electron transfer distance. This distance can be considerably shorter than the geometrical metal–metal separation when significant electronic coupling exists. By using the iron–chromium distance in **1**$^+$**–5**$^+$ obtained by DFT calculations, we estimate a lower limit of H_{ab} (Table 5). The delocalisation coefficient α quantifies the fraction of valence electronic charge transferred from the donor to the acceptor metal centres. For an unsymmetrical Class II mixed-valence species the thermal barrier $\Delta G^{\ddagger}$ is given by Eq. (5) [18]

$$\Delta G^{\ddagger} = \frac{\lambda}{4} + \frac{E_0}{2} + \frac{E_0^2}{4(\lambda - 2H_{ab})} - H_{ab} + \frac{H_{ab}^2}{(\lambda + E_0)} \quad (5)$$

The electron transfer parameters, H_{ab}, α, and $\Delta G^{\neq}$ are characteristic of weakly coupled Class II mixed-valence systems. In particular, the values of the thermal barrier to the electron transfer reveal that the rate increases in the order **1**$^+$ < **2**$^+$ < **3**$^+$ < **4**$^+$ < **5**$^+$ in the range 10^1–10^4 s^{-1}.

The optical energy $E_{op} = \tilde{\nu}_{max}$ of an IT band is related to the electrochemical potential difference ΔE by Eq. (6) [9,10]

$$\tilde{\nu}_{max} = \Delta E + \Delta E' + \lambda \quad (6)$$

Here, $\Delta E'$ represents the difference between the $Fe^{II/III}$ oxidation potential with the oxidized (indene)$Cr(CO)_3$ and the measured $Fe^{II/III}$ potential, and λ the reorganisational energy. On the basis of the oxidation potential for **6P**/**6P**$^+$, **2P**/**2P**$^+$ and **3P**/**3P**$^+$ (*vide supra*) $\Delta E'$ can be reasonably approximated as 60 mV when the ferrocenyl is in 2-position, and almost null in 3-position. Provided that λ is constant, a plot of $\tilde{\nu}_{max}$ versus $E_0 = (\Delta E + \Delta E')$ is linear and this occurs for the **1**$^+$**–5**$^+$ series (except **1**$^+$), the only variable being the position and the indene methylation. The least square fit of the data (Fig. 10) gave a slope of 0.91 ± 0.11 with $R = 0.9995$ in good agreement with the theoretical value of unit.

An inspection of the molecular structures along the series **1**-**5** reveals that the non correlation of **1**$^+$ can be interpreted on the basis of the *transoid* conformation of the metal groups in **1** in contrast with the *cisoid* conformation in the other complexes. Assuming that the same conformations are maintained in the cations and in solution, the reorganisational energy λ for *transoid* **1**$^+$ should be substantially higher than those for *cisoid* cations. As a consequence, the optical energy ($\tilde{\nu}_{max}$) of the near-IR transition is expected to be higher and the correlation fails for **1**$^+$.

The molar absorption coefficient (ε_{max}) of the IT bands in the oxidised complexes **1**$^+$**–5**$^+$ (Table 5) increases by decreasing E_0. For a Gaussian shaped peak the oscillator strength (f) is related to ε_{max} and can be experimentally determined by using Eq. (7) where $\Delta\tilde{\nu}_{1/2}$ represents the half-band width [16d,17a]

$$f = (4.6 \times 10^{-9})\varepsilon_{max}\Delta\tilde{\nu}_{1/2} \quad (7)$$

A quite good trend of f with E_0 within the series of the cations **1**$^+$**–5**$^+$ (except **4**$^+$ which partially decomposes during the acquisition) is found (Fig. 11).

This behaviour clearly indicates that the smaller E_0 is, the greater the oscillator strength in the charge transfer transition results.

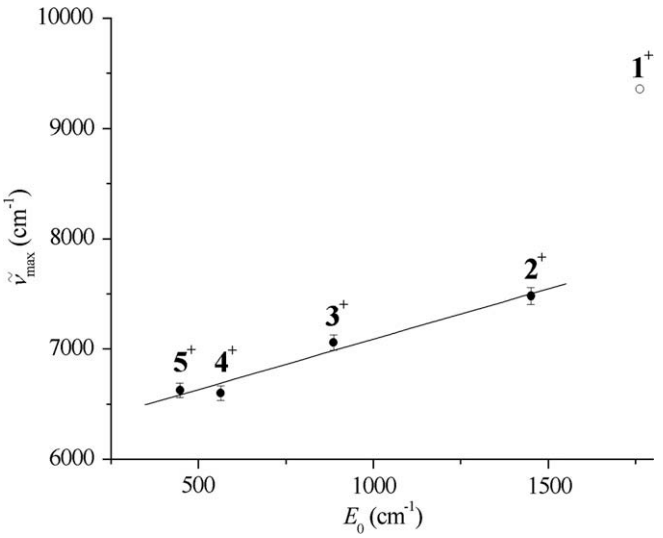

Fig. 10. Optical energy ($\tilde{\nu}_{max}$) of the near-IR transition vs. E_0 for **1**$^+$**–5**$^+$.

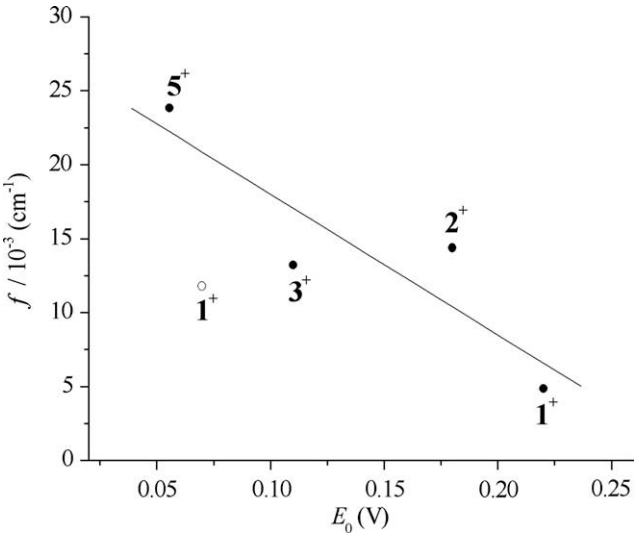

Fig. 11. Oscillator strength (f) of near-IR transition vs. E_0 for **1**$^+$–**5**$^+$.

On the basis of the linear correlation of both $\tilde{\nu}_{max}$ and f with E_0 it follows that more efficient charge transfer corresponds to smaller E_0. Similar correlations have been previously observed for other LMCT transitions in Fc-conjugated cations [19]. In particular, the dependence of f from E_0 very recently found by us for the corresponding series of (ferrocenyl)indenes [6] is reinforced along **1**$^+$–**5**$^+$. Actually, the slope of the linear plot is much higher in the heterobimetallic series (0.095) than in the corresponding monometallic series (0.04).

2.6. DFT analysis

The molecular electronic features of **1** and **2** have been previously described by means of DFT calculations [4]. The present computational analysis describes the mixed-valence isomers **1**$^+$ and **2**$^+$. The effect of the presence of methyl substituents in the indenyl ring, which has been recently investigated in detail in some ferrocenyl precursors [6], is theoretically explored in **3**, **4** and **5** and in their charged derivatives, which were found to display larger stability than **1**$^+$ and **2**$^+$ complexes.

The radical cations **1**$^+$ and **2**$^+$, obtained by full optimization of **1** and **2** reducing their electron count by one to mimic the effects of oxidation, do not exhibit significant structural difference when compared to their neutral precursors. The most relevant calculated interatomic distances and angles are reported in Table 2, using the numbering scheme reported in Fig. 1. Upon oxidation when going from **2** to **2**$^+$ the distances between Fe and the centroids of the coordinated Cp rings, Q_1 and Q_2, increase by approximately 0.04 Å. In contrast, the increase of the distance between Cr and the centre of the benzene moiety Q is smaller (0.02 Å). The average distance between Cr and the CO ancillary ligands increases by 0.02 Å, suggesting that these bonds in the cation are more labile and their substitution is easier, as experimentally found [8]. It is worth noting that these variations are predicted in all the couples neutral complex/radical cation of the present study. In fact, analogous, albeit less enhanced structural changes are computed also when going from **1** to **1**$^+$ (Table 2). No peculiar deformations of the bridging ligand are observed, as expected, since the HOMOs of both **1** and **2** are strongly iron d orbitals centered (Table 2).

The geometry of the dication **2**$^{2+}$ converged with triplet multiplicity. Both the distances Fe—$Q_{1,2}$ and Cr—Q increase by about 0.04 Å with respect to **2**$^+$ with concerted lengthening of the Cr–CO bonds (Table 2). Any attempt to obtain **1**$^{2+}$ failed at the employed level of theory.

Full geometry optimization starting from the couple of crystallographic structures **3** and **3**′ was carried out (Table 2); **3** was found energetically more stable and was used as starting point to compute the geometry of the radical cation **3**$^+$. The presence of the methyl groups induces significant torsion of the bridging ligand about the bond C4–C14, but the metals, which are disposed in *cisoid* conformation are closer by approximately 0.2 Å than in **1**.

The relevant geometric parameters computed for **4** and **5** and reported in Table 2 are very similar, the latter molecular structure being in good agreement with the crystallographic data, except in the distances involving chromium. In fact the Cr–benzene interaction is fairly diffuse [20] and is the part of the molecule most sensitive to basis set choice and electron correlation. As stated above, upon oxidation increase of the distances Fe—$Q_{1,2}$ Cr—Q and Cr—CO is predicted analogous to that observed in the non-methylated isomers **2**/**2**$^+$ (Table 2). Interestingly, the geometries of the dicationic species **4**$^{2+}$ and **5**$^{2+}$ converged both as triplet and as singlet, but the calculations do not indicate significant differences between the structural parameters optimised for the two spin state configurations (Table 2). In addition the two electronic states are energetically close.

The trend of the adiabatic first ionization potentials nicely reflects the trend of the $E_{1/2}$ of the voltammetric first wave: **4** < **5** < **3** < **2** < **1**. In Table 6 the metal d percentage composition of the frontier Kohn–Sham MOs is reported. The HOMOs have significant contribution of Fe d orbitals (above 60%); Cr d orbitals percentage contribution is found in the HOMOs of **2**, **4** and **5**, i.e. in the isomers with the "linear" bridge. The Fe/Cr d orbitals contribution to the LUMOs drastically diminishes (less than 25%); in fact the LUMOs are mainly composed by carbon p(π) lobes. The topological features of the frontier MOs of **1**–**5** and the energy gaps

Table 6
Fe and Cr metal d orbitals percentage composition of the frontier Kohn–Sham MOs of complexes **1–5**

		Fe d_{xy}	Fe d_{xz}	Fe d_{yz}	Fe $d_{x^2-y^2}$	Fe d_{z^2}	Cr d_{xy}	Cr d_{xz}	Cr d_{yz}	Cr $d_{x^2-y^2}$	Cr d_{z^2}	Fe_{tot}	Cr_{tot}
1	H	15.1	12.2	15.4	24.0	11.4	–	–	–	–	–	78.1	–
	L	1.1	3.4	–	2.1	–	1.7	1.0	–	1.3	–	6.6	4.0
2	H	–	1.4	19.5	34.5	16.1	–	4.0	–	–	–	77.9	4.0
	L	5.2	3.6	–	6.2	1.9	–	–	–	–	–	16.9	–
3	H	17.8	*1.4*	*17.0*	–	*41.2*	–	––	–	–	–	77.4	–
	L	–	*6.5*	*1.4*	–	*3.1*	–	–	–	–	1.2	11.0	1.2
3′	H	8.2	*6.0*	–	*13.8*	*51.6*	–	–	–	–	–	79.6	–
	L	–	–	–	–	–	–	3.5	–	–	–	–	3.5
4	H	2.0	36.5	6.4	7.5	9.3	–	–	1.2	3.3	7.0	61.7	11.5
	L	8.5	5.9	4.4	–	–	2.2	–	–	1.2	1.5	18.8	4.9
5	H	–	1.5	17.2	33.6	14.1	–	6.9	–	–	–	66.4	6.9
	L	5.8	5.2	–	6.8	1.6	1.1	4.0	–	–	–	19.4	5.1

Table 7
Energy gaps (eV) between frontier Kohn–Sham MOs

	HOMO–LUMO	HOMOα–LUMOα	HOMOβ–LUMOβ
1	2.154	–	–
1^{+}	–	2.273	0.071
2	1.968	–	–
2^{+}	–	2.069	0.240
2^{2+}**(T)**	–	2.274	0.267
3	2.182	–	–
3′	2.354	–	–
3^{+}	–	2.266	0.107
4	1.986	–	–
4^{+}	–	2.153	0.215
4^{2+}**(T)**	–	2.082	0.469
4^{2+}**(S)**	–	0.710	0.569
5	2.009	–	–
5^{+}	–	2.050	0.271
5^{2+}**(T)**	–	2.084	0.498
5^{2+}**(S)**	–	0.573	0.686

Table 8
Voronoi charges and Mulliken spin densities

	Voronoi charge		Spin density	
	Fe	Cr	Fe	Cr
1	−0.076	0.298	–	–
1^{+}	−0.015	0.310	0.6598	0.3460
2	−0.071	0.298	–	–
2^{+}	−0.008	0.313	0.6901	0.3774
2^{2+}**(T)**	0.043	0.341	1.1647	0.8734
3	−0.075	0.299	–	–
3′	−0.070	0.298	–	–
3^{+}	−0.019	0.313	0.6074	0.3978
4	−0.070	0.298	–	–
4^{+}	−0.018	0.317	0.6021	0.4418
4^{2+}**(T)**	0.043	0.341	1.1451	0.9096
4^{2+}**(S)**	0.043	0.341	1.1335	−0.9032
5	−0.070	0.298	–	–
5^{+}	−0.014	0.315	0.6320	0.3759
5^{2+}**(T)**	0.043	0.341	1.1352	0.9081
5^{2+}**(S)**	0.041	0.341	−1.1041	0.8814

(Table 7) allow to assign with confidence the lowest energy absorptions that occur in the visible region of these neutral complexes to metal-to-ligand charge transfer (MLCT) bands.

Upon oxidation mixing of the levels occurs and the topology of the Kohn–Sham frontier MOs changes significantly. For oxidized open-shell species the analysis of the Voronoi charges and of the spin densities distributions, which are reported in Table 8, is useful to probe the delocalization of the unpaired electron(s). The iron center is calculated to be electron-rich relative to the chromium center to a less extent in the monooxidized complexes than in their neutral precursors. The evolution of the charges in the cations and dications indicate that both metals lose electron density upon oxidation, as expected. In all the studied radical cations most of the spin density is asymmetrically localized on the metal centers, a picture consistent with trapped valence behaviour. The ratios spin density on iron / spin density on chromium are: **4**$^{+}$ (1.36) < **3**$^{+}$ (1.53) < **5**$^{+}$ (1.68) < **2**$^{+}$ (1.83) < **1**$^{+}$ (1.91). It is clear that the spin density on chromium is larger in the methylated ions than in **1**$^{+}$ and **2**$^{+}$.

Table 9
Calculated excitation energies, oscillator strengths and assignment for the mixed-valence complexes **2**$^{+}$ and **5**$^{+}$

	Transitions		Oscillator strength	Excitation energy (eV/cm^{-1})	Assignment
2^{+}	98α → 102α	0.107			
	101α → 102α	−0.206	0.024	1.212/9780	MMCT
	101α → 104α	0.104			
	95β → 101β	0.180			
	97β → 101β	−0.118			
	100β → 101β	0.961			
	100β → 102β	0.107			
5^{+}	122α → 126α	−0.134			
	125α → 126α	−0.264	0.029	1.171/9445	MMCT
	119β → 125β	0.260			
	121β → 125β	0.142			
	124β → 125β	0.933			

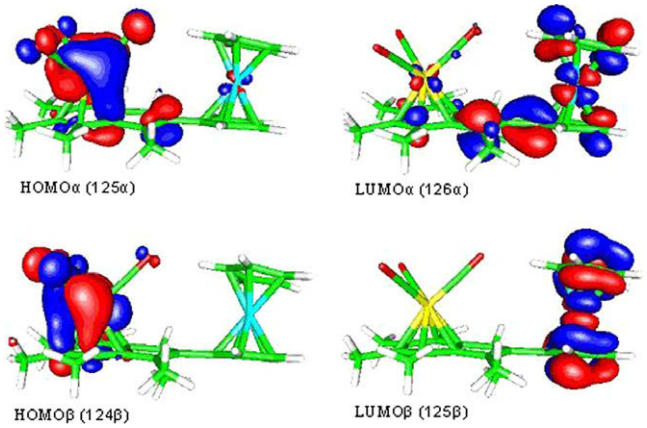

Fig. 12. Kohn–Sham molecular spin orbitals involved in the main monoelectronic transitions contributing to the near-IR absorption of **5**$^{+}$.

The interpretation of the spectroscopic near-IR absorption and the assignment of the electronic transitions was explored by TD-DFT approach at PCM-B3LYP/LANL2DZ, 6-31G** level of theory (see Section 4.8) for **2**$^{+}$ and **5**$^{+}$. The calculated excitation energies are reported in Table 9 together with their assignment and oscillator strengths. The main contribution comes both for **2**$^{+}$ and for **5**$^{+}$ from the monoelectronic transitions HOMOβ → LUMOβ and HOMOα → LUMOα. These molecular spin orbitals are shown in Fig. 12 for complex **5**$^{+}$. The nature of the near-IR absorption can be clearly assigned to a chromium-to-iron charge transfer band (MMCT).

3. Conclusions

The evaluation of the electronic communication between two metal sites necessitates the assemblage of different experimental techniques supported by computational investigation. This work combines the structural parameters with the electrochemical data, the reactivity, and the analysis of the IT transition in the near-IR of a series of heterobimetallic η^6-[(ferrocenyl)indene]-Cr(CO)$_3$ complexes differing from the position of the ferrocenyl group and the degree of indene methylation. Moreover it has been enriched with computational results.

The outcomes reported herein provide important experimental evidence that "redox matching" of donor and acceptor oxidation potentials results in greater electronic coupling. Furthermore, we have demonstrated that **1**$^{+}$**–5**$^{+}$ are electrochromic systems in which $\tilde{\nu}_{max}$ can be predicted for the redox asymmetry E_0 and the absorption band in the near-IR can be switched on and off by the ferrocenyl redox couple.

This is a rare example of linear correlation of the energy and oscillator strengths of the near-IR transition with E_0 for a series of heterobimetallic complexes. TD-DFT calculations indicate that

the nature of the near-IR absorption can be clearly assigned to a chromium-to-iron charge transfer band.

Finally, Hush analysis has allowed to estimate the values of the thermal barrier of the electron transfer evidencing that the rate of the metal-to-metal electron transfer increases in the order $\mathbf{1^+ < 2^+ < 3^+ < 4^+ < 5^+}$.

4. Experimental

4.1. General procedure

All reactions and complex manipulations were performed in an oxygen and moisture-free atmosphere utilizing standard Schlenk techniques or in a Mecaplex glovebox. Solvents were dried by reflux over the appropriate drying agent and distilled under stream of argon. Acetylferrocenium tetrafluoroborate was prepared following the procedure previously reported [21].

4.2. General procedure for the synthesis of [η^6-(ferrocenyl) indenes]-$Cr(CO)_3$ (**1–5**)

Complexes [η^6-(3-ferrocenyl)-1,2,4,5,6,7-hexamethylindene]-$Cr(CO)_3$ (**3**), [η^6-(2-ferrocenyl)-4,5,6,7-tetramethylindene]-$Cr(CO)_3$ (**4**), and [η^6-(2-ferrocenyl)-1,3,4,5,6,7-hexamethylindene]-$Cr(CO)_3$ (**5**), were prepared by using the same procedure previously described for the synthesis of [η^6-(3-ferrocenyl)-indene]-$Cr(CO)_3$ (**1**) and [η^6-(2-ferrocenyl)-indene]-$Cr(CO)_3$ (**2**) [4] starting from the corresponding ferrocenyl-indenes [6].

[η^6-(3-Ferrocenyl)-1,2,4,5,6,7-hexamethylindene]-$Cr(CO)_3$ (**3**): $Cr(CO)_6$ (0.4 g, 1.8 mmol), CH_3CN (20 mL), (3-ferrocenyl)hexamethylindene (0.384 g, 1.0 mmol) and THF (20 mL) were used as starting materials for the synthesis of **3** (0.281 g, 0.54 mmol, 58%). Crystals suitable for X-ray analysis were grown from slow diffusion of *n*-hexane into CH_2Cl_2 solution at −30 °C.

^{1}H NMR (400.13 MHz, CD_2Cl_2, δ ppm, 298 K, TMS): δ 4.67 (m, 1H, $H_{\alpha'}$), 4.30 (m, 2H, H_β, $H_{\beta'}$), 4.25 (m, 1H, H_α), 4.19 (s, 5H, Cp), 3.43 (q, 1H, J(H, CH_3) = 7 Hz, H1), 2.44 (s, 3H, 2-CH_3), 2.25 (s, 3H, 6-CH_3), 2.34 (s, 3H, 7-CH_3), 2.09 (s, 3H, 5-CH_3), 1.93 (s, 3H, 4-CH_3), 1.30 (d, 3H, J(H, CH_3) = 7 Hz, 1-CH_3). ^{13}C NMR (100.61 MHz, CD_2Cl_2, δ ppm, 298 K, TMS): δ 236.32 ($Cr(CO)_3$), 148.45 (C2), 131.18 (C3), 120.66 (C7a), 112.18 (C3a), 106.98 (C5), 105.89 (C4, C6), 104.11 (C7), 82.69 (Cj), 71,85 ($C_{\alpha'}$), 71.62 (C_α), 67.58 ($C_{\beta'}$), 69.91 (CCp), 66.77 (C_β), 47.89 (C1), 17.81 (4-CH_3), 17.35 (7-CH_3) 17.11 (1-CH_3), 16.84 (5-CH_3), 16.14 (6-CH_3), 15.31 (2-CH_3). Anal. Calc. for $C_{28}H_{28}CrO_3Fe$: C, 64.63; H, 5.42. Found: C, 64.92; H, 5.51%.

[η^6-(2-Ferrocenyl)-4,5,6,7-tetramethylindene]-$Cr(CO)_3$ (**4**): $Cr(CO)_6$ (0.4 g, 1.8 mmol), CH_3CN (20 mL), (2-ferrocenyl)tetramethylindene (0.356 g, 1.0 mmol) and THF (20 mL) were used as starting materials for the synthesis of **4** (0.197 g, 0.4 mmol, 40%).

^{1}H NMR (400.13 MHz, CD_2Cl_2, δ ppm, 298 K, TMS): δ 6.61 (m, 1H, H3), 4.58 (m, 1H, $H_{\alpha'}$), 4.49 (m, 1H, H_α), 4.38 (m, 1H, $H_{\beta'}$), 4.36 (m, 1H, H_β), 4.17 (s, 5H, Cp), 3.71–3.80 (q AB, 2H, J(H, H) = 22 Hz, $H1_{endo}$, $H1_{exo}$), 2.37 (s, 3H, 7-CH_3), 2.35 (s, 3H, 4-CH_3), 2.24 (s, 3H, 6-CH_3), 2.23 (s, 3H, 5-CH_3). ^{13}C NMR (100.61 MHz, CD_2Cl_2, δ ppm, 298 K, TMS): δ 119.71 (C3), 119.57 (C2), 116.77 (C3a), 111.48 (C7a), 106.92 (C5), 105.10 (C6), 104.53 (C7), 101.10 (C4), 69.77 (C_β, $C_{\beta'}$), 69.71 (CCp), 67.03 (C_α), 66.30 ($C_{\alpha'}$), 40.19 (C1), 16.28 (4-CH_3, 7-CH_3), 15.81 (5-CH_3, 6-CH_3). Anal. Calc. for $C_{26}H_{24}CrO_3Fe$: C, 63.43; H, 4.91. Found: C, 63.81; H, 5.39%.

[η^6-(2-ferrocenyl)-1,3,4,5,6,7-hexamethylindene]-$Cr(CO)_3$ (**5**): $Cr(CO)_6$ (0.4 g, 1.8 mmol), CH_3CN (20 mL), (2-ferrocenyl)hexamethylindene (0.384 g, 1.0 mmol) and THF (20 mL) were used as starting materials for the synthesis of **5**. From purification of the crude product by MPLC were obtained the two isomers (1-*endo*-CH_3)-[η^6-(2-ferrocenyl)-1,3,4,5,6,7-hexamethylindene]-$Cr(CO)_3$(**5**-*endo*) (42 mg, 0.08 mmol, 8%) and (1-*exo*-CH_3)-[η^6-(2-ferrocenyl)-1,3,4,5,6,7-hexamethylindene]-$Cr(CO)_3$ (**5**-*exo*) (0.224 g, 0.43 mmol, 43%) using petroleum ether/diethyl ether (80:20) as eluent. Crystals suitable for X-ray analysis of the complex **5**-*exo* were grown from slow diffusion of *n*-hexane into CH_2Cl_2 solution at −30 °C.

5-*endo*. ^{1}H NMR (400.13 MHz, CD_2Cl_2, δ ppm, 298 K, TMS): δ 4.51 (m, 1H, $H_{\alpha'}$), 4.43 (m, 1H, H_α), 4.37 (m, 2H, H_β, $H_{\beta'}$), 4.14 (s, 5H, Cp), 3.60 (q, 1H, J(H, CH_3) = 7 Hz, H1), 2.51 (s, 3H, 3-CH_3), 2.47 (s, 3H, 4-CH_3), 2.38 (s, 3H, 7-CH_3), 2.32 (s, 3H, 5-CH_3), 2.17 (s, 3H, 6-CH_3), 1.41(d, 3H, J(H, CH_3) = 7 Hz, 1-CH_3). ^{13}C NMR (100.61 MHz, CD_2Cl_2, δ ppm, 298 K, TMS): δ 236.52 ($Cr(CO)_3$), 150.06 (C2), 130.98 (C3), 120.77 (C3a), 118.04 (C7a), 111.55 (C5), 109.51 (C7), 101.50 (C6), 97.99 (C4), 79,70 (Cγ), 70.88 (C'_α), 69,70 (CCp), 69.45 (C'_β), 69.00 (C_β), 68.56 (C_α), 45.29 (C1), 22.98 (1-CH_3), 16.65 (4-CH_3), 16.56 (3-CH_3), 16.52 (5-CH_3), 16.44 (6-CH_3), 16.12 (7-CH_3). Anal. Calc. for $C_{28}H_{28}CrO_3Fe$: C, 64.63; H, 5.42. Found: C, 64.66; H, 5.58%.

5-*exo* .^{1}H NMR (400.13 MHz, CD_2Cl_2, δ ppm, 298 K, TMS): δ 4.38 (m, 1H, H_α), 4.49 (m, 1H, $H_{\alpha'}$), 4.35 (m, 2H, H_β, $H_{\beta'}$), 4.19 (s, 5H, Cp), 3.71 (q, 1H, J(H, CH_3) = 7 Hz, H1), 2.53 (s, 3H, 4-CH_3), 2.50 (s, 3H, 3-CH_3), 2.39 (s, 3H, 7-CH_3), 2.26 (s, 3H, 6-CH_3), 2.22 (s, 3H, 5-CH_3), 1.20 (d, 3H, J(H, CH_3) = 7 Hz, 1-CH_3). ^{13}C NMR (100.61 MHz, CD_2Cl_2, δ ppm, 298 K, TMS): δ 236.32 ($Cr(CO)_3$), 147.91 (C2), 130.71 (C3), 119.75 (C7a), 114.12 (C3a), 107.84 (C5), 106.45 (C6), 103.77 (C7), 103.66 (C4), 79.58 (Cγ), 70.04 ($C_{\alpha'}$), 69.65 (C_β), 68.59 ($C_{\beta'}$), 69.61 (CCp), 68.46 (C_α), 45.70 (C1), 18.31 (1-CH_3), 17.32 (7-CH_3), 16.62 (3-CH_3), 16.50 (5-CH_3), 16.27 (6-CH_3), 16.09 (4-CH_3). Anal. Calc. for $C_{28}H_{28}CrO_3Fe$: C, 64.63; H, 5.42. Found: C, 64.83; H, 5.35%.

4.3. Synthesis of [[η^6-(3-ferrocenyl)-indene]-$Cr(CO)_2[P(OEt)_3]_2][BF_4]_2$, **[1P$_2$][BF$_4$]$_2$**, [$\eta^6$-(2-ferrocenyl)-indene]-$Cr(CO)_2[P(OEt)_3]_2][BF_4]_2$, **[2P$_2$][BF$_4$]$_2$** and [$\eta^6$-(1,2,3,4,5,6,7-heptamethyl)-indene]-$Cr(CO)_2[P(OEt)_3]_2][BF_4]_2$, **[7P$_2$][BF$_4$]$_2$**

Complexes **[1P$_2$][BF$_4$]$_2$**, **[2P$_2$][BF$_4$]$_2$** and **[7P$_2$][BF$_4$]$_2$** were prepared with the same method previously described by Sweigart et al. [8] for the synthesis of [[η^6-(ferrocenyl)-benzene]-$Cr(CO)_2[P(OEt)_3]_2$].

[1P$_2$][BF$_4$]$_2$: $P(OEt)_3$ (0.13 mL), **1** (50 mg, 0.11 mmol), acetylferrocenium tetrafluoroborate (69 mg, 0.22 mmol) and CH_2Cl_2 (8 mL) were used as starting materials for the synthesis of **[1P$_2$][BF$_4$]$_2$** (24 mg,0.026 mmol, 24%).

^{1}H NMR (400.13 MHz, CD_2Cl_2, δ ppm, 298 K, TMS): δ 7.48 (4H, Ar), 7.17 (1H, H2), 4.74 (2H, H_α, $H_{\alpha'}$), 4.50 (2H, H_β, $H_{\beta'}$), 4.20 (5H, Cp), 4.11 (12H, OCH_2), 3.89 (1H, H1), 3.67 (1H, H1), 1.50 (18H, OCH_3). ^{31}P NMR (161.98 MHz, CD_2Cl_2, δ ppm, 298 K, H_3PO_4 (85%)): δ 159.7.

[2P$_2$][BF$_4$]$_2$: $P(OEt)_3$ (0.13 mL), **2** (50 mg, 0.11 mmol), acetylferrocenium tetrafluoroborate (69 mg, 0.22 mmol) and CH_2Cl_2 (8 mL) were used as starting materials for the synthesis of **[2P$_2$][BF$_4$]$_2$** (64 mg, 0.07 mmol, 64%).

^{1}H NMR (400.13 MHz, CD_2Cl_2, δ ppm, 298 K, TMS): δ 6.62 (4H, Ar), 6.34 (1H, H3), 4.78 (4H, H_α, $H_{\alpha'}$, H_β, $H_{\beta'}$), 4.36 (5H, Cp), 4.24 (12H, OCH_2), 3.92 (2H, H1), 1.47 (18H, OCH_3). ^{31}P NMR (161.98 MHz, CD_2Cl_2, δ ppm, 298 K, H_3PO_4 (85%)): δ 161.8.

[7P$_2$][BF$_4$]$_2$: $P(OEt)_3$ (0.13 mL), **7** (38 mg, 0.11 mmol), acetylferrocenium tetrafluoroborate (69 mg, 0.22 mmol) and CH_2Cl_2 (8 mL) were used as starting materials for the synthesis of **[7P$_2$][BF$_4$]$_2$** (18 mg,0.022 mmol, 20%).

^{1}H NMR (400.13 MHz, CD_2Cl_2, δ ppm, 298 K, TMS): δ 4.23 (12H, OCH_2), 3.60 (1H, H1), 2.67–2.16 (18H, CH_3 Ar, 2-CH_3, 3-CH_3), 1.39 (3H, 1-CH_3), 1.26 (18H, OCH_3). ^{31}P NMR (161.98 MHz, CD_2Cl_2, δ ppm, 298 K, H_3PO_4 (85%)): δ 164.3.

4.4. X-ray crystallography

The X-ray structures were obtained by collecting the intensities data at room temperature using a Philips PW1100 single-crystal diffractometer (FEBO system) using a graphite-monochromated (Mo Kα) radiation, following the standard procedures. All intensities were corrected for Lorentz polarization and absorption [22a]. The structure was solved by direct methods using SIR-97 [22b]. Refinement was carried out by full-matrix least-squares procedures (based on F_o^2) using anisotropic temperature factors for all non-hydrogen atoms. The H-atoms were placed in calculated positions with fixed, isotropic thermal parameters ($1.2\,U_{equiv}$ of the parent carbon atom). The calculations were performed with the SHELXL-97 program [22c] implemented in the WINGX package [22d]. IR spectra were recorded on a Bruker Equinox 55 FT-IR spectrometer.

4.5. NMR analysis

^{1}H and ^{13}C NMR spectra were obtained on a Bruker Avance DRX spectrometer ($T = 298$ K) operating at 400.13 and 100.61 MHz, respectively. The assignments of the proton resonances were performed by standard chemical shift correlation and NOESY experiments. The ^{13}C resonances were attributed through 2D-heterocorrelated COSY experiments (HMQC [23a] using pulsed field gradients for coherence and quadrature detection in F1 achieved by using the TPPI method [23b–d] for the H-bonded carbon atoms, HMBC [23e,f] for the quaternary ones).

4.6. Electrochemistry and spectroelectrochemistry

CV experiments were performed in an air-tight three electrode cell connected to a vacuum/argon line. The reference electrode was a SCE (Tacussel ECS C10) separated from the solution by a bridge compartment filled with the same solvent/supporting electrolyte solution used in the cell. The counter electrode was a platinum spiral with ca. 1 cm^2 apparent surface area. The working electrodes were disks obtained from cross section of gold wires of different diameters (0.5, 0.125 and 0.025 mm) sealed in glass. Between successive CV scans the working electrodes were polished on alumina according to standard procedures and sonicated before use. An EG&G PAR-175 signal generator was used. The currents and potentials were recorded on a Lecroy 9310L oscilloscope. The potentiostat was home-built with positive feedback loop for compensation of ohmic drop [24]. Mid-IR, near-IR and visible spectroelectrochemistry experiments at variable temperatures were carried out with a cryostated (low-T) Optically Transparent Thin-Layer Electrochemical (OTTLE) cell (IDEAS!UvA B.V., University of Amsterdam, The Netherlands) [25] equipped with CaF_2 windows. Pt working (80% transmittance), Pt auxiliary minigrid electrodes, and pseudo-reference Ag wire are melt-sealed in the insulating polyethylene spacer with optical path of 0.023 cm.

4.7. EPR spectroscopy

EPR spectra were recorded using a Bruker ECS 106 X-band spectrometer equipped with a standard TE_{102} rectangular cavity and an Oxford Instrument ESR-900 helium flow cryostat. EPR experimental conditions were as follows: temperature, 10 K or 150 K; microwave frequency, 9.4 GHz, microwave power, 20 mW, modulation amplitude, 10 Gauss.

The oxidized species were generated by adding acetylferrocenium tetrafluoroborate (1.0 equiv.) to a CH_2Cl_2 solution of the neutral complexes (2 mM) at 228 K. After stirring for 10 min 200 μL of reaction mixture were quickly transferred by cannula into an EPR tube, which was immediately frozen in liquid nitrogen.

4.8. Computational details

Density functional theory (DFT) calculations were carried out using the Amsterdam density functional (ADF) program [26]. Electron correlation was treated within the local density approximation (LDA) in the Vosko-Wilk-Nusair parametrisation [27] and the non-local corrections of Becke [28] and Perdew [29] were added to the exchange and correlation energies. The basis set used for the atoms in the optimisation procedures are TZP (triple-χ Slater-type orbital (STO) basis, extended with a single-z polarization function) for H, frozen core up to 2p for Fe and Cr, frozen core up to 1s for C and O. Single point calculations were subsequently carried out on the optimised geometries employing TZ2P basis set (triple-STO basis, extended with a double-z polarization function) for H, frozen core up to 2p for Fe and Cr, frozen core up to 1s for C and O and the results obtained with this basis set are reported in the tables and discussed in the text.

Spin contamination in the open-shell calculations was carefully monitored to assess the reliability of the wavefunction.

Excitation energies were calculated using TD-DFT implemented in GAUSSIAN03 [30]. The hybrid B3LYP functional was employed. Standard LANL2DZ-ECP [31] basis sets were used for the metal nuclei, 6-31G** [31] was employed for O, C and H (B3LYP/LANL2DZ, 6-31G**). Solvent effects were modelled with PCM [32]. A standard cavity was used and the parameters for dichloromethane were chosen $\varepsilon = 2.02$ and $r = 2.27$ Å.

Supplementary material

CCDC 694519, 694520 and 694521 contain the supplementary crystallographic data for 3(c), 3′(d) and 5(f). These data can be obtained free of charge from The Cambridge Crystallographic Data Centre via www.ccdc.cam.ac.uk/data_request/cif.

Acknowledgements

This work was supported by the Ministero dell'Istruzione, dell'Università e della Ricerca (MUR) within PRAT 2006. CINECA (Consorzio di calcolo del Nord-Est, Casalecchio di Reno) is gratefully acknowledged for the access to the computational facilities, i.e. IBM SP5.

References

[1] (a) R.G. Rocha, F.N. Rein, H. Jude, A.P. Shreve, J.J. Concepcion, T.J. Meyer, Angew. Chem., Int. Ed. 47 (2008) 503;
(b) W. Kaim, G.K. Lahiri, Angew. Chem., Int. Ed. 46 (2007) 1778;
(c) D.M. D'Alessandro, F.R. Keene, Chem. Rev. 106 (2006) 2270;
(d) J.-P. Launay, Chem. Soc. Rev. 30 (2001) 386;
(e) S. Barlow, D. O'Hare, Chem. Rev. 97 (1997) 637.
[2] (a) C.G. de-Azevedo, K.P.C. Vollhardt, Synlett (2002) 1019;
(b) C.G. Atwood, W.E. Geiger, J. Am. Chem. Soc. 122 (2000) 5477;
(c) H. Schottenberger, M. Buchmeiser, C. Rieker, P. Jaitner, K. Wurst, J. Organomet. Chem. 541 (1997) 249;
(d) P.A. McGovern, K.P.C. Vollhardt, Synlett (1990) 493;
(e) M.-H. Desbois, D. Astruc, J. Guillin, J.-P. Mariot, F. Varret, J. Am. Chem. Soc. 107 (1985) 5280;
(f) N.G. Connelly, A.R. Lucy, J.D. Payne, A.M.R. Galas, W.E. Geiger, J. Chem. Soc., Dalton Trans. (1983) 1879;
(g) E.W. Neuse, M.S. Loonat, Trans. Met. Chem. 6 (1981) 260;
(h) C. LeVanda, K. Bechgaard, D.O. Cowan, M.D. Rausch, J. Am. Chem. Soc. 99 (1977) 296.
[3] (a) N. Wheatley, P. Kalck, Chem. Rev. 99 (1999) 3379;
(b) A. Ceccon, S. Santi, L. Orian, A. Bisello, Coord. Chem. Rev. 248 (2004) 683.
[4] S. Santi, A. Ceccon, A. Bisello, C. Durante, P. Ganis, L. Orian, F. Benetollo, L. Crociani, Organometallics 24 (2005) 4691.
[5] E.L. Muetterties, J.R. Bleeke, E.J. Wucherer, T.A. Albright, Chem. Rev. 82 (1982) 499.
[6] S. Santi, L. Orian, A. Donoli, C. Durante, A. Bisello, P. Ganis, A. Ceccon, L. Crociani, F. Benetollo, Organometallics 26 (2007) 5867.
[7] D.E. Richardson, H. Taube, Coord. Chem. Rev. 60 (1984) 107.

[8] L.K. Yeung, J.E. Kim, D.Y.K. Chung, P.H. Rieger, A. Sweigart, Organometallics 15 (1996) 3891.
[9] J.W. Merkert, W.E. Gelger, M.N. Paddon-Row, A.M. Oliver, A.L. Rheingold, Organometallics 11 (1992) 4109.
[10] M. Moran, I. Cuadrado, M.C. Pascual, C.C. Casado, Organometallics 11 (1992) 1210.
[11] A. Garg, D.M. Nemer, H. Choi, J.B. Sheridan, W.E. Geiger, Organometallics 25 (2006) 275.
[12] J.S. Miller, D.T. Glatzhofer, C. Vazques, R.S. McLean, J.C. Calabrese, W.J. Marshall, J.W. Raebiger, Inorg. Chem. 40 (2001) 2058.
[13] J.M. Manriquez, M.D. Ward, W.M. Reiff, J.C. Calabrese, N.L. Jones, P.J. Carrol, E.E. Bunel, J.S. Miller, J. Am. Chem. Soc. 117 (1995) 6182.
[14] C. Elsechenbroich, J. Hech, J. Am. Chem. Soc. 101 (1979) 6773.
[15] T-Y. Dong, D.N. Kambara, D.N. Hendrickson, J. Am. Chem. Soc. 108 (1986) 4423.
[16] (a) C.C. Allen, N.S. Hush, Prog. Inorg. Chem. 8 (1967) 357;
(b) M.B. Robin, P. Day, Adv. Inorg. Chem. Radiochem. 10 (1967) 247;
(c) C. Creutz, Prog. Inorg. Chem. 30 (1983) 1;
(d) R.J. Crutchley, Adv. Inorg. Chem. 41 (1994) 273.
[17] (a) N.S. Hush, Prog. Inorg. Chem. 8 (1967) 391;
(b) K.D. Demadis, C.M. Haertshorn, T.J. Meyer, Chem. Rev. 101 (2001) 2655;
(c) B.S. Brunschwig, C. Creutz, N. Sutin, Chem. Soc. Rev. 31 (2002) 168;
(d) D.M. D'Alessandro, F.R. Keene, Chem. Soc. Rev. 35 (2006) 424.
[18] B.S. Brunschwig, N. Sutin, Coord. Chem. Rev. 187 (1999) 233.
[19] (a) A.H. Flood, C.J. McAdam, K.C. Gordon, H.G. Kjaergaard, A.M. Manning, B.H. Robinson, J. Simpson, Polyhedron 26 (2007) 448;
(b) L. Cuffe, D.A. Richard, R.D.A. Hudson, G.F. Gallagher, S. Jennings, C.J. McAdam, R.B.T. Connely, A.M. Manning, B.H. Robinson, J. Simpson, Organometallics 24 (2005) 2051;
(c) Y. Zhu, M.O. Wolf, J. Am. Chem. Soc. 122 (2000) 10121.
[20] A.A. Low, M.B. Hall, Int. J. Quantum Chem. 77 (2000) 152.
[21] N.G. Connelly, W.E. Geiger, Chem. Rev. 96 (1996) 877.
[22] (a) A.T.C. North, D.C. Philips, F.S. Mathews, Acta Crystallogr. A 24 (1968) 351;
(b) A. Altomare, M.C. Burla, M. Camalli, G.L. Cascarano, C. Giacovazzo, A. Guagliardi, A.G.G. Moliterni, G. Polidori, R. Spagna, SIR-97, J. Appl. Crystallogr. 32 (1999) 115;
(c) G.M. Sheldrick, SHELXL-97, Program for the Refinement of Crystal Structures, University of Göttingen, Germany, 1997;
(d) L.J. Farrugia, J. Appl. Crystallogr. 32 (1999) 837.
[23] (a) A. Bax, S. Subramanian, J. Magn. Reson. 67 (1986) 565;
(b) T. Parella, Magn. Reson. Chem. 36 (1998) 467;
(c) J. Ruiz-Cabello, G.W. Vuister, C.T.W. Moonen, P. van Gelderen, J.S. Cohen, P. van Zijl, J. Magn. Reson. 100 (1992) 282;
(d) W. Willker, D. Leibfritz, R. Kerrsebaum, W. Bermel, Magn. Reson. Chem. 31 (1993) 287;
(e) A. Bax, M.F. Summers, J. Am. Chem. Soc. 108 (1986) 2093;
(f) M.F. Summers, L.G. Marzilli, A. Bax, J. Am. Chem. Soc. 108 (1986) 4285.
[24] C. Amatore, C. Lefron, F. Pflüger, J. Elecroanal. Chem. 270 (1989) 43.
[25] (a) F. Hartl, H. Luyten, H.A. Nieuwenhuis, G.C. Schoemaker, Appl. Spectrosc. 48 (1994) 1522;
(b) T. Mahabiersing, H. Luyten, R.C. Nieuwendam, F. Hartl, Collect. Czech., Chem. Commun. 68 (2003) 1687.
[26] (a) G. te Velde, F.M. Bickelhaupt, S.J.A. van Gisbergen, C. Fonseca Guerra, E.J. Baerends, J.G. Snijders, T. Ziegler, J. Comput. Chem. 22 (2001) 931;
(b) C. Fonseca Guerra, J.G. Snijders, G. te Velde, E.J. Baerends, Theor. Chem. Acc. 99 (1998) 391;
(c) ADF 2007.01, SCM, Theoretical Chemistry, Vrije Universiteit, Amsterdam, The Netherlands, <http://www.scm.com>.
[27] S.D. Vosko, L. Wilk, M. Nusair, Can. J. Chem. 58 (1990) 1200.
[28] (a) A.D. Becke, J. Chem. Phys. 84 (1986) 4524;
(b) A.D. Becke, Phys. Rev. A 38 (1988) 3098.
[29] (a) J.P. Perdew, Phys. Rev. B 33 (1986) 8822;
(b) J.P. Perdew, Phys. Rev. B 34 (1986) 7406.
[30] GAUSSIAN 03, Revision B.05, M.J. Frisch, G.W. Trucks, H.B. Schlegel, G.E. Scuseria, M. A. Robb, J.R. Cheeseman, J.A. Montgomery Jr., T. Vreven, K.N. Kudin, J.C. Burant, J.M. Millam, S.S. Iyengar, J. Tomasi, V. Barone, B. Mennucci, M. Cossi, G. Scalmani, N. Rega, G.A. Petersson, H. Nakatsuji, M. Hada, M. Ehara, K. Toyota, R. Fukuda, J. Hasegawa, M. Ishida, T. Nakajima, Y. Honda, O. Kitao, H. Nakai, M. Klene, X. Li, J.E. Knox, H.P. Hratchian, J.B. Cross, V. Bakken, C. Adamo, J. Jaramillo, R. Gomperts, R.E. Stratmann, O. Yazyev, A.J. Austin, R. Cammi, C. Pomelli, J.W. Ochterski, P.Y. Ayala, K. Morokuma, G.A. Voth, P. Salvador, J.J. Dannenberg, V.G. Zakrzewski, S. Dapprich, A.D. Daniels, M.C. Strain, O. Farkas, D.K. Malick, A.D. Rabuck, K. Raghavachari, J.B. Foresman, J.V. Ortiz, Q. Cui, A.G. Baboul, S. Clifford, J. Cioslowski, B.B. Stefanov, G. Liu, A. Liashenko, P. Piskorz, I. Komaromi, R.L. Martin, D.J. Fox, T. Keith, M.A. Al-Laham, C.Y. Peng, A. Nanayakkara, M. Challacombe, P.M. W. Gill, B. Johnson, W. Chen, M.W. Wong, C. Gonzalez, J.A. Pople, GAUSSIAN, Inc., Wallingford CT, 2004.
[31] (a) Basis sets were obtained from the Extensible Computational Chemistry Environment Basis Set Database, Version 02/25/04, as developed and distributed by the Molecular Science Computing Facility, Environmental and Molecular Sciences Laboratory which is part of the Pacific Northwest Laboratory, P.O. Box 999, Richland, Washington 99352, USA, and funded by the US Department of Energy. The Pacific Northwest Laboratory is a multi-program laboratory operated by Battelle Memorial Institute for the US Department of Energy under contract DE-AC06-76RLO 1830. P.J. Hay, W.R. Wadt, J. Chem. Phys. 82 (1985) 270;
(b) P.J. Hay, W.R. Wadt, J. Chem. Phys. 82 (1985) 284;
(c) P.J. Hay, W.R. Wadt, J. Chem. Phys. 82 (1985) 299.
[32] (a) E. Cancès, B. Mennucci, J. Tomasi, J. Chem. Phys. 107 (1997) 3032;
(b) B. Mennucci, E. Cancès, J. Tomasi, J. Phys. Chem. B 101 (1997) 10506;
(c) S. Miertus, E. Scrocco, J. Tomasi, Chem. Phys. 55 (1981) 117.